MICRO ROTARY BALL BEARING WITH INTEGRATED BALL CAGE: FABRICATION AND CHARACTERIZATION

Robert Hergert, Ingrid S.Y. Ku, Tom Reddyhoff, and Andrew S. Holmes
Imperial College London, UK

ABSTRACT

This paper presents a rotary MEMS ball bearing with an integrated silicon ball cage. The device is a deep groove radial ball bearing consisting of steel balls encapsulated between two micromachined silicon wafers. The silicon ball cage is released from the bulk silicon substrate during fabrication. The objective was to show that a simple caged bearing design provides reliable motion at both high and low speeds. The running torque of two identical devices was measured for speeds ranging from 10 to 20,000 rpm. One of the devices was disassembled before failure to provide images of the wear experienced during testing.

INTRODUCTION

Reliable rotary MEMS devices require a long lasting and mechanically stable bearing. We propose that micro-ball bearings could provide the solution to both of these problems. Ball bearings have been widely used in macro scale devices since the industrial revolution, and they offer potential advantages over other more established MEMS scale bearings. They can provide greater longevity and higher speed operation than pin-joint bearings [1], while being more stable and easier to control than magnetic levitation bearings [2]. Ball bearings can also operate reliably at lower speeds and have a less complex design than air bearings such as those described in [3]. Ghodssi et al. have recently demonstrated the effectiveness of micro ball bearings in MEMS devices [4, 5, 6]. As discussed in [4], one of the problems encountered in current designs is the tendency for the balls to co-locate or jam in the bearing raceway. We have addressed this problem by integrating a ball cage in our design.

We have created a set of prototype devices to test the silicon cage structure. The current design uses 500μm-diameter steel balls and three lithographic masks. The steel balls are sandwiched between two pieces of micromachined silicon, which are bonded together using electrodeposited solder. The silicon cage is released from the bulk substrate after soldering. The process flow is presented in more detailed below.

Testing is performed on a custom microtribology rig described below. The bearing is placed into a micromachined silicon platform, which is used to measure running torque. It is then coupled to a servomotor, which provides the normal load and rotational force. The speed of the motor can be precisely controlled between 10 and 20,000 rpm.

Running torque measurements are reported for two similar devices and our results show that the caged bearing can withstand speeds of up to 20,000 rpm, which is the upper limit for the current testing configuration. The first device was tested for more than 3 hours and survived speeds of up to 19,000 rpm. At this point the solder bonds on the cage failed. The second device survived 5 hours of continuous testing and speeds up to 20,000 rpm. This device was disassembled before failure to evaluate the wear experienced during testing.

DESIGN

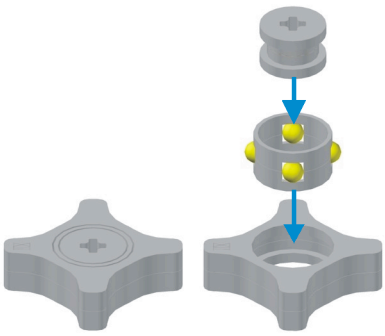

Figure 1 - CAD rendering of an assembled bearing with ball cage (left) and exploded diagram showing all of the individual parts (right).

Figure 1 shows a CAD rendering of the bearing design. In the exploded diagram on the right the top part is the bearing rotor. The middle part represents the ball cage with the steel balls in the cage openings. Both of these parts fit into the stator, at the bottom, which is designed to fit into a torque testing device. All of the pieces, with the exception of the steel balls, are fabricated from a silicon substrate. The bearing is fabricated in two halves, which are held together with solder bonds.

The devices reported here use 500μm steel balls. The outer diameter of the bearing track is 2.2mm with a cage thickness of 100μm. A 10μm tolerance was designed into the ball track and the arms of the cage, which means that the rotor has the freedom to move up to 20μm laterally. A 40μm gap was used on either of side of cage to release it from the stator.

978-1-4244-5764-9/10/$26.00 ©2010 IEEE

The rotor has a diameter of 1.18mm. These dimensions are illustrated in Figure 2. This design was chosen for testing due to the high yield during fabrication. Also, the 10µm tolerance allows for greater misalignment while coupling the motor to the device during testing.

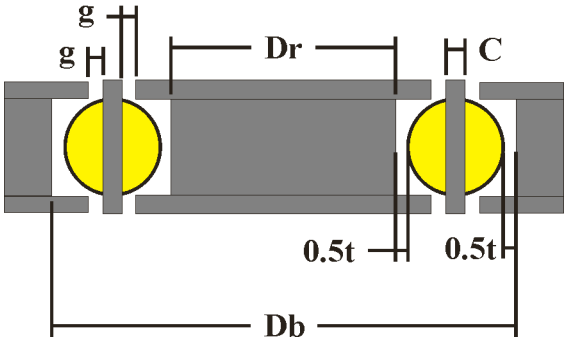

Figure 2 - Depiction of the bearing design parameters: g - cage release gap (40µm), C – cage width (100µm), t – raceway tolerance (10µm), Dr – rotor diameter (1.18mm), Db – bearing raceway diameter (2.2mm).

FABRICATION

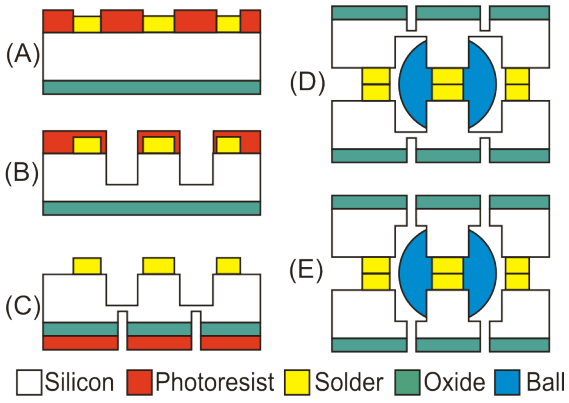

Figure 3 - Microfabrication process flow (A) Electrodeposition of solder layer; (B) DRIE deep etching of ball raceway; (C) Backside oxide patterning and partial release etch using DRIE; (D) Insertion of steel balls, alignment of matching parts, and solder bonding; (E) Rotor and cage release by double side shallow DRIE using pre-patterned oxide mask.

Figure 3 shows the simplified process flow for the devices. This process requires only 3 lithographic masks. The first step is to pattern plate the solder layer. This is done on a sputtered seed layer of chrome and copper. The solder layer consists of 3µm of nickel, 3µm of tin, and 200nm of gold. The bearing raceway and the cage arms are then patterned using silicon deep reactive ion etching (DRIE). The raceway etch is controlled by carefully monitoring the etch depth. Due to variations in etch depth across the wafer we aim for an over etch of approximately 5µm, giving a nominal bearing raceway trench depth of 255µm. The backside of the wafer is then patterned with the cage release features. This requires patterning a 500nm oxide layer that will be used as a mask in the final processing step, then using DRIE to etch a further 230µm. At this point the wafer is split into individual dies for soldering. Each die contains five bearings. The steel balls are manually placed in the bearing raceway between the cage arms. We then paint solder flux onto the solder points on one of the die. This is done because we are currently performing the soldering in a non-reducing environment and the flux greatly improves the reflow process. Corresponding die are then visually aligned on a custom aligner/ bonder. Pressure is applied to the die and it is rapidly heated to form the solder bonds. After bonding each side of the device is released using DRIE. Figure 4 shows SEM images of the fabricated bearing parts.

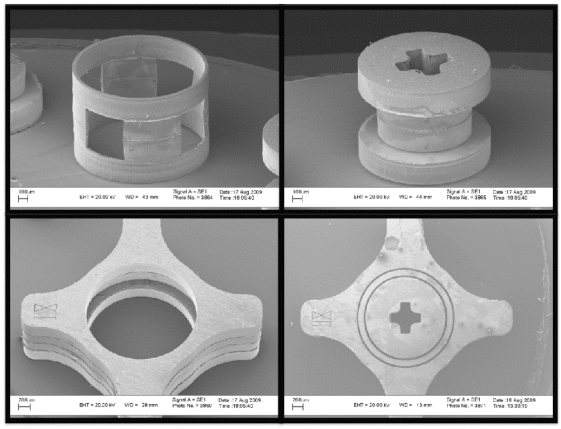

Figure 4 - SEM images of the micromachined bearing parts: ball cage (top left), rotor (top right), stator (bottom left) and fully assembled device (bottom right).

In the current fabrication process some damage is occurring to the raceway during the DRIE release step, as illustrated in Figure 5. We are exploring methods to minimize or eliminate this effect.

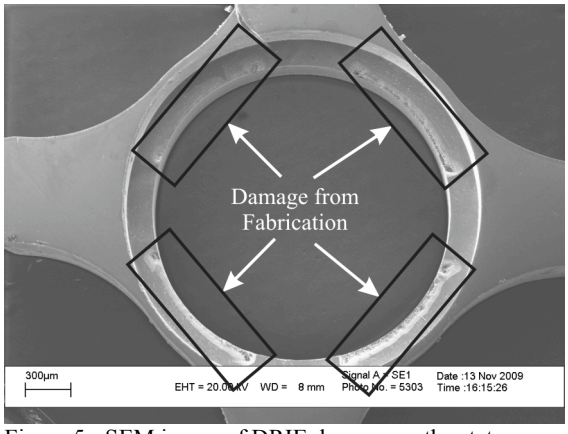

Figure 5 - SEM image of DRIE damage on the stator. Similar damage is present on the rotor.

TEST SETUP

Prototype ball bearings have been characterized in a custom microtribology test rig developed at Imperial College. A full description of the measurement setup can be found in [7]. The rig allows the measurement of the frictional torque of the ball bearing under varying normal loads and over a range of rotational speeds. The outer part of the bearing is mounted in a silicon micromachined test platform incorporating an elastic suspension (see Figure 6), while the inner part is coupled to the shaft of a precision motor, which provides both normal force and rotation. Optical techniques are used to measure the out-of-plane displacement of the sample holder, and its in-plane rotation. The applied normal load and running torque are determined from these displacements, using the known spring constants of the suspension.

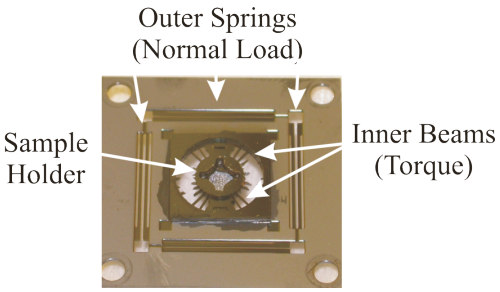

Figure 6 - Micromachined test platform. Outer springs are used to determine normal load; inner platform beams are used to measure applied torque.

The limitation of this testing arrangement is that we can only measure the axial normal load and not the radial load on the bearing. However, this does provide the opportunity to stress test the device using the least ideal load configuration for a radial deep groove bearing.

RESULTS

Initial testing shows that the bearings perform well at both high and low speeds. Testing was carried out on two devices at speeds ranging from 10 to 20,000 rpm with a 60mN axial load. The motor used during testing limited the maximum speed. The torque profile for the devices conforms to the expected torque curve. At lower speeds the torque will decrease as the balls move from sliding and stick/slip to rolling friction. Figure 8 shows the average of three low speed torque measurements for both tested bearings. As the graph indicates, the torque generally decreased with increasing speed between 10 and 550 rpm. Both devices showed a decrease from around 15 μNm at 50 rpm to 2 μNm at 550 rpm.

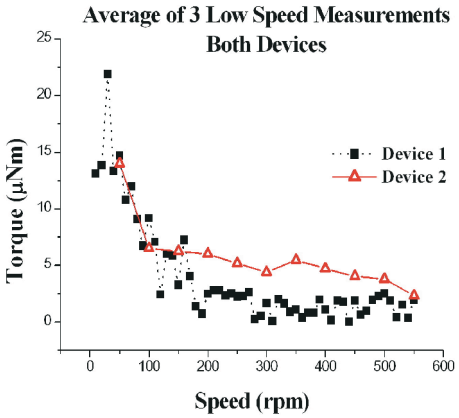

Figure 7 - Average of 3 low speed measurements for each device.

At much higher speeds we would expect to see an increase in the measured torque. Figure 8 shows an average of three high speed measurements for the second device. There is a general decreases in torque at speeds from 1000 – 9000 rpm and a gradual increase at speeds above 9000 rpm. The test rig was not configured correctly during high speed testing of the first device making the measurements unreliable. Retesting was not possible due to device failure. Therefore the results are not presented here.

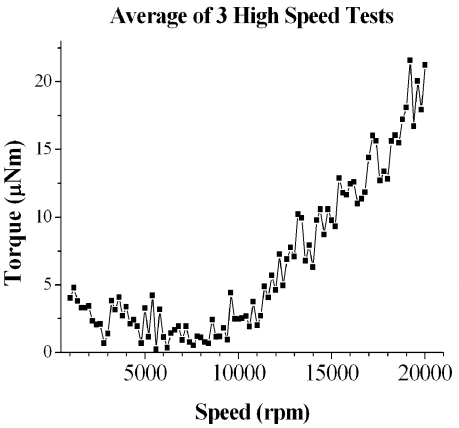

Figure 8 -Torque measurements from three high speed tests on the second device.

After 5 hours of continuous testing, we debonded the second device to evaluate the wear at the contact points between the steel balls and the silicon cage and raceway. Figures 9 to 11 show that there was relatively little wear of the silicon structures during testing. The first device failed after 3 hours of testing due to poor adhesion between the solder and the silicon arms of the cage. This indicates that the weakest point in the current design is the solder bond between the arms of the

ball cage. The longevity of the bearing could be improved by improving the strength of this bond using a different fabrication process, or by designing the cage such that a bond is not needed.

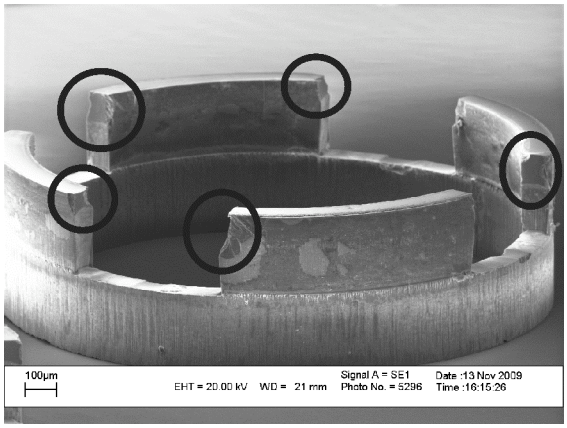

Figure 9 - SEM image showing the wear on one half of the ball cage. Wear areas enclosed in the circles are the lateral contact points of the steel balls.

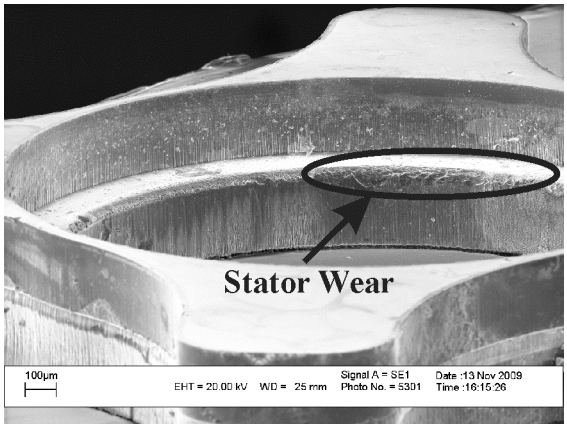

Figure 10 - SEM image showing the wear on the bottom half of the silicon stator. Damage contained in the ellipse is due to wear; the other damage is due to fabrication.

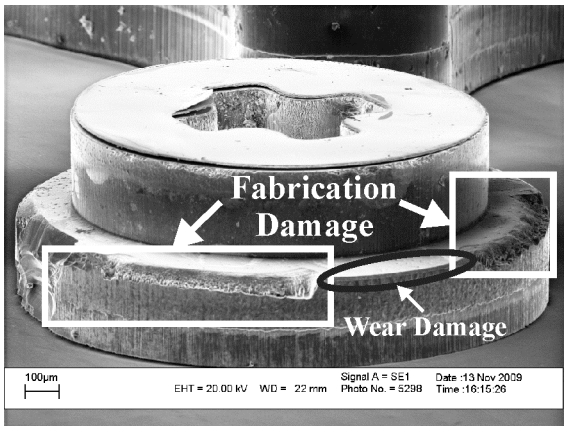

Figure 11 - SEM image showing wear on the top half of the silicon rotor. Fabrication damage is highlighted in the boxes and wear damage is contained in the ellipse.

CONCLUSION

We have shown that an encapsulated ball bearing with an integrated ball cage can perform reliably between 10 and 20,000 rpm. The current design shows relatively minimal silicon wear after several hours of continuous operation. A closer evaluation of the fabrication damage and the testing wear will need to be carried out determine the causes of the raceway damage. These initial results seem to indicate that a micro ball bearing with an integrated cage could provide a stable platform for rotary MEMS devices at both high and low speeds. However, longevity and higher speed testing would provide a clearer picture of the durability and applicability of the design.

REFERENCES

[1] D. M. Tanner, J. A. Walraven, S. S. Mani, S. E. Swanson, “Pin-joint design effect on the reliability of a polysilicon microengine,” Proc. of IRPS, pp. 122-129, 2002.

[2] S. Lee, K. Daejong, M.D. Bryant, F.F. Ling, “A micro corona motor,” Sensors and Actuators: A. Physical, vol. 118, No. 2, pp. 226-232, 28 Feb., 2005.

[3] S. Tanaka, Y. Miura, P. Kang, et al., “MEMS-based air turbine with radial-inflow type journal bearing,” IEEJ Trans on Electrical and Electronic Engineering, vol. 3, No. 3, pp. 297-304, 2008.

[4] C. M. Waits, B. Geil, R. Ghodssi, "Encapsulated Ball Bearings for Rotary Micro Machines," Journal of Micromechanics and Microengineering (JMM), vol. 17, pp. S224-S229, August 2007.

[5] M. McCarthy, C. M. Waits, and R. Ghodssi, "Dynamic Friction and Wear in a Planar-Contact Encapsulated Microball Bearing using an Integrated Microturbine," Journal of Microelectromechanical Systems (JMEMS), vol. 18, No. 2, pp. 263-273, April 2009.

[6] M. McCarthy, C. M. Waits, M. I. Beyaz, and R. Ghodssi, "A Rotary Microactuator Supported on Encapsulated Microball Bearings Using an Electro-pneumatic Thrust Balance," Journal of Micromechanics and Microengineering (JMM), vol. 19, pp. 1095-1098, August 2009.

[7] I.S.Y. Ku, T. Reddyhoff, J.H. Choo, A.S. Holmes, H.A. Spikes, “A novel tribometer for the measurement of friction in MEMS,” Tribology International, in press.